Research Square

Preprints are preliminary reports that have not undergone peer review.
They should not be considered conclusive, used to inform clinical practice,
or referenced by the media as validated information.

Comparative In Vitro Effects of Direct Non-Thermal Plasma and Plasma-Activated Medium on U87-MG Glioblastoma and L-929 Fibroblast Cells

Elham Sadat Mousavi
Laser and Plasma Research Institute, Shahid Beheshti University
Mohsen Rahmanian
North Khorasan University of Medical Sciences
Fatemeh Oroojalian
North Khorasan University of Medical Sciences
Reza Fallah
University of Birjand
Sara Khosropanah
North Khorasan University of Medical Sciences
Seyed Mohammad Khorashadizadeh
University of Birjand
Amir Rahmanian Sharifabad
rahmanian_Amir@yahoo.com

North Khorasan University of Medical Sciences

Article

Keywords: Glioblastoma, Differential Cellular Response, MTT Assay, Non-Thermal Plasma, Plasma-Activated Medium

Posted Date: September 23rd, 2026

DOI: https://doi.org/10.21203/rs.3.rs-11117669/v1

License: This work is licensed under a Creative Commons Attribution 4.0 International License.
Read Full License

Additional Declarations: No competing interests reported.

Abstract

Non-thermal plasma (NTP) and plasma-activated medium (PAM) are being investigated as redox-based approaches for glioblastoma. In this manuscript, PAM denotes plasma-treated sterile deionized water subsequently added to complete culture medium. We compared direct NTP exposure and PAM treatment in human U87-MG glioblastoma and murine L-929 fibroblast cells. Direct NTP exposure was applied for 30, 60, or 90 s at a device output setting of 200 V. PAM was tested as undiluted stock (100%) and as 50%, 25%, and 12.5% stock conditions; 10 µL was added to 150 µL of complete medium. MTT-derived metabolic activity was assessed after 72 h. Each condition comprised 24 technical wells within a single plate-based experimental run. Direct NTP exposure for 60 and 90 s reduced MTT absorbance in both cell lines, whereas 30 s produced no clear change. Undiluted PAM stock reduced MTT absorbance in U87-MG cells, whereas the lower PAM stock conditions did not.

Introduction

Glioblastoma, classified as a grade 4 primary brain tumor by the World Health Organization, remains the most aggressive and lethal malignancy of the central nervous system in adults(1). Originating from neuroglial stem or progenitor cells, glioblastoma is associated with a profoundly poor prognosis, conferring both a high mortality rate and a severe impact on patient quality of life(2). Despite decades of research and advances in neuro-oncology, the standard of care—which includes maximal safe surgical resection, followed by radiotherapy and chemotherapy with temozolomide—only modestly extends survival, with median overall survival times typically under two years and long-term remission remaining rare. The biological complexity of glioblastoma, characterized by rapid proliferation, diffuse infiltration, and remarkable heterogeneity at both the genetic and cellular levels, underlies its formidable resistance to current therapies. Moreover, treatment is further complicated by the presence of a robust blood–brain barrier (BBB) and blood–tumor barrier, an immunosuppressive tumor microenvironment, high vascularity, and the persistence of cancer stem cell populations, all of which enable tumor recurrence and drive resistance to conventional and novel therapeutics. These multifaceted challenges make glioblastoma a paradigm of therapeutic difficulty in modern neuro-oncology, underscoring the urgent need for innovative and more effective treatment strategies(3).

Glioblastoma resists therapy through a convergent network of molecular, epigenetic, and microenvironmental programs that maintain stemness, enable adaptive signaling, and shield against cytotoxic stress. Chromatin remodeling enzymes such as EZH2, PRMTs, and KDM5A sustain therapy-resistant transcriptional states, while ATRX loss and alternative telomere lengthening confer replicative resilience. Oncogenic rewiring via EGFRvIII–RAS–PI3K and PDGFRA pathways, reinforced by transcriptional regulators like FOXG1 and SOX9, drives bypass signaling and lineage plasticity. Concurrently, metabolic adaptation under hypoxia—marked by lipid metabolic reprogramming and extracellular matrix (ECM) remodeling—induces resistance to radiotherapy and promotes immunosuppression. These hypoxic niches are further enriched with immune-evasive myeloid cells and PD-1/PD-L1 signaling, collectively forming a stem-like, metabolically flexible, and immunosuppressive

tumor ecosystem. This systems-level integration of genomic instability, adaptive signaling, and environmental crosstalk renders glioblastoma uniquely refractory to conventional therapies (4).

The development of novel approaches to glioblastoma therapy is critically important given the profound resistance of glioblastoma stem cell subpopulations to conventional treatment modalities(5). Non-thermal plasma (NTP), also known as cold atmospheric plasma (CAP), exerts its biological and anti-tumor effects primarily through the generation of reactive oxygen species (ROS) and reactive nitrogen species (RNS), collectively termed RONS (6). These plasma-generated RONS are capable of diffusing into cells and triggering a cascade of biochemical events—including oxidative modifications of proteins, lipids, and nucleic acids—that disrupt cellular homeostasis and induce cell death(6). The selectivity of CAP for tumor cells over normal cells is largely attributed to differences in cell membrane composition—particularly the lower cholesterol content and higher aquaporin expression in cancer cells—which increases their permeability to RONS and susceptibility to oxidative damage(6). Once inside, excessive RONS overwhelm the tumor cell's antioxidant defenses, increase intracellular calcium, trigger mitochondrial dysfunction, activate mitogen-activated protein kinase (MAPK) cascades, and inflict DNA damage—all converging on apoptosis or other forms of cell death(6, 7). Furthermore, CAP-treated tumor cells frequently release damage-associated molecular patterns (DAMPs), which can trigger immunogenic cell death (ICD) and thereby engage the innate and adaptive immune system — a feature that could potentially augment anti-tumor immunity beyond the directly exposed tumor cells (8).

Thus, the anti-cancer action of NTP is fundamentally mediated by the controlled delivery of ROS and RNS, which exploit the vulnerabilities of malignant cells to oxidative stress while largely sparing normal tissues(6). At the core of CAP/NTP's anti-tumor activity lies the production of a complex mixture of reactive oxygen species (ROS) and reactive nitrogen species (RNS), which together generate a potent oxidative/nitrosative stress in target cells. Upon exposure to CAP — whether through direct plasma jets or via plasma-activated medium (PAM) — short-lived radicals (e.g., superoxide anion $O_2{\cdot}^-$, hydroxyl radical ·OH, singlet oxygen $^1O_2$), longer-lived species (hydrogen peroxide H_2O_2, nitrite/nitrate, nitric oxide NO), and secondary reactive species (e.g., peroxynitrite $ONOO^-$) are generated (8). These reactive species can diffuse across the extracellular milieu, and — aided by cell membrane features such as upregulated aquaporins and altered lipid composition in many cancer cells — they traverse into the cytoplasm (9). Once internalized, RONS overwhelm cellular antioxidant systems (e.g., glutathione, catalase), leading to depletion of glutathione pools and inactivation of protective catalase activity on the cell membrane (10). In this manuscript, PAM denotes plasma-treated sterile deionized water subsequently added to complete culture medium.

CAP can be applied either directly — exposing cells or tissues to the plasma jet or discharge — or indirectly via liquid media treated with CAP, commonly termed plasma-activated medium (PAM). Direct plasma treatment delivers both the reactive chemical species (ROS/RNS) and physical components (charged particles, ultraviolet (UV) photons, electromagnetic fields) simultaneously to the target cells. Physical factors (e.g., electromagnetic emissions) have been suggested to contribute to cytotoxic effects beyond pure chemical oxidative stress, potentially enabling trans-barrier, "contactless"

cytotoxicity in settings where direct plasma cannot reach deeper tissues (11). In contrast, PAM relies solely on the long-lived reactive species (e.g., hydrogen peroxide, nitrite/nitrate, other stable ROS/RNS) dissolved in liquid, delivering a chemically defined but simpler redox insult to cells (10).

Empirical comparisons across multiple studies suggest that direct CAP treatment often induces more immediate and extensive cell death than PAM under comparable conditions. For example, experiments in murine melanoma models observed greater tumor-cell kill and larger reduction of tumor volume with direct CAP relative to PAM, especially in in vivo settings (12). However, PAM retains significant advantages, particularly in translational contexts: as a liquid, it can be injected or perfused, reaching deeper or otherwise inaccessible tumor regions, making it more suitable for internal or deep-seated tumors (13). Additionally, PAM produces less collateral physical stress (no UV, charged particles, or strong electromagnetic fields), which may translate into reduced risk to surrounding normal tissues — a critical consideration for sensitive tissues such as the brain or areas protected by the blood-brain barrier. Indeed, review articles note that plasma-treated liquids are among the most advanced plasma-medicine modalities for applying CAP's anticancer potential in vivo (14).

To compare the cellular response patterns produced by direct and liquid-mediated plasma treatment, the present study evaluated human U87-MG glioblastoma cells and murine L-929 fibroblast cells within a harmonized experimental framework. Cells were exposed to graded durations of direct NTP or serial dilutions of PAM under matched culture and assay conditions. The primary endpoint was MTT-derived metabolic activity; therefore, apoptosis, proliferation, and clonogenic survival were not directly measured. We hypothesized that direct NTP and PAM would produce distinct exposure-dependent MTT response patterns in the two cell lines.

Methods

Materials

The materials utilized in this study included high-glucose Dulbecco's Modified Eagle Medium (DMEM; 4.5 g/L) sourced from GIBCO, along with fetal bovine serum (FBS) and Penicillin-Streptomycin (Pen-Strep) from BIOSERA (supplied by Denazist). Phosphate-buffered saline (PBS) was obtained from DNABIOTECH. The human glioblastoma cell line U87-MG and the murine fibroblast cell line L-929 were obtained from the Institute of Biotechnology at Ferdowsi University of Mashhad, Iran.

For cell detachment, Trypsin 10X was acquired from Sigma-Aldrich (supplied by Denazist). Sterile deionized water from Damavand was used for plasma activation and serial dilutions. Non-thermal plasma was generated using a Satya dielectric barrier discharge device equipped with stainless-steel electrodes and a needle-type plasma applicator. According to the device specifications, the power supply operated from a 220 V AC input and provided a sinusoidal AC output adjustable from 0 to 30 kV at a frequency of 20 kHz, with a maximum rated output power of 500 W. The mean electron density specified for the plasma was approximately 1×10^{15} cm^{-3}. Spectrophotometric measurements were performed using a StatFax 2100 ELISA reader.

All culture-grade plasticware was of analytical grade, including T25 flasks from JETBIOFIL, 96-well plates from LABSELECT, and microbial plates from SPL. Additional laboratory consumables included 15 mL and 50 mL Falcon tubes from Maat Kariz Mehr, 1.5 mL microtubes and various pipette tips (blue, yellow, and crystal) from TRUSTMOMED, 96% ethanol from Pars Alcohol, and sterile gauze from Zarin Teb.

Cell culture

Human U87-MG glioblastoma cells and murine L-929 fibroblast cells were cultured under standard conditions using high-glucose Dulbecco's Modified Eagle Medium (DMEM; 4.5 g/L glucose) supplemented with 10% fetal bovine serum (FBS). Cultures were maintained at 37°C in a humidified atmosphere containing 5% CO_2. Prior to experimental manipulation, cell viability and membrane integrity were verified by Trypan Blue exclusion. For all plasma-based treatments, 15,000 cells per well were seeded into 96-well flat-bottom polystyrene plates (well diameter ≈ 6.94 mm) in 150 µL of complete medium. Following seeding, cells were incubated for 24 hours to allow for attachment and equilibration prior to exposure.

Experimental layout and replication scheme

For each reported treatment condition, n = 24 represented technical replicate wells obtained within a single plate-based experimental run. The experiment was not independently repeated on different days, and the 24 wells did not constitute independent biological replicates. Treatment and control wells were spatially interleaved to reduce the possibility of unintended exposure of adjacent wells. Accordingly, the statistical analyses describe within-experiment well-level variation and should not be interpreted as evidence of between-experiment reproducibility.

Direct non-thermal plasma exposure protocol

Direct NTP exposure was performed using a custom-fabricated Satya DBD device equipped with stainless-steel electrodes and a needle-type plasma applicator. Ambient atmospheric air was used as the working gas without an externally supplied gas stream; consequently, no gas flow rate was set. The plasma applicator was positioned perpendicular to the sample surface at a distance of 2 cm. Because the discharge was needle-type, a defined circular plasma diameter or treatment footprint was not measured.

For direct treatment, the device was operated at the output setting reported as 200 V, and the cells were exposed for 30, 60, or 90 seconds. No independent voltage measurement was performed across the discharge; therefore, the reported 200 V value represents the device setting rather than the measured discharge voltage. The device had a maximum rated output power of 500 W; however, the actual power delivered to the samples under the selected operating condition was not independently measured. According to the device specifications, the mean electron density was approximately 1×10^{15} cm^{-3}; this parameter was not independently measured during the present experiments. To confine the plasma stream and mitigate off-target exposure to adjacent wells, the setup used a quartz isolation conduit

(outer diameter: 7 mm; length: 2 cm) mechanically interfaced with a custom-machined stainless-steel alignment plate. The guide plate contained 7 mm apertures matched to the dimensions and spacing of the well format.

PAM generation and handling

PAM was generated by exposing 5 mL aliquots of sterile deionized water contained in standard 6-well tissue-culture plates to the previously described needle-type plasma source. Treatment was performed under ambient atmospheric air without an externally supplied gas flow, with a constant distance of 2 cm between the plasma applicator and the liquid surface.

PAM was generated using three device output settings reported as 100, 200, and 300 V and two treatment durations of 5 and 10 minutes, yielding six generation conditions. These voltage values represented device settings and were not independently measured across the discharge.

Following treatment, all PAM preparations were immediately transferred for spectrophotometric evaluation using a StatFax 2100 ELISA reader over the 200–300 nm ultraviolet range. Among the tested conditions, PAM generated using the device output setting reported as 200 V for 5 minutes produced the selected ultraviolet absorbance profile, with a primary absorbance maximum at 215 nm (1.85 absorbance units) and a minimum at 260 nm (0.021 absorbance units). This condition was selected as the standard PAM formulation for subsequent experiments. The liquid-surface temperature was monitored during plasma treatment. No measurable reduction in liquid volume was observed following either 5 or 10 minutes of plasma exposure. The freshly generated PAM was used immediately after treatment and was not stored before its addition to the cell cultures.

The PAM stock was used undiluted (100%) or diluted with untreated sterile deionized water to produce the 50%, 25%, and 12.5% PAM stock conditions. Ten microliters of each PAM stock condition were immediately added to wells containing 150 µL of complete culture medium. These conditions corresponded to final treated-liquid fractions of 6.25%, 3.125%, 1.5625%, and 0.78125% (v/v), respectively, in the final well volume of 160 µL. Vehicle-control wells received 10 µL of untreated sterile deionized water.

MTT assay

Cellular viability following experimental intervention was quantitatively evaluated at the 72-hour post-treatment interval using the MTT (3-[4,5-dimethylthiazol-2-yl]-2,5-diphenyl tetrazolium bromide) colorimetric assay, which measures the reduction of the tetrazolium compound as an indirect index of mitochondrial metabolic activity. Following incubation, culture media were carefully aspirated to eliminate extracellular by-products, and monolayers were gently rinsed with 200 µL of sterile 1X phosphate-buffered saline (PBS) in order to remove residual serum proteins and unattached cells.

Subsequently, 50 µL of MTT solution at a concentration of 5 mg/mL was dispensed into each well under sterile conditions, and the plates were incubated for four hours at 37°C in a humidified incubator to

facilitate intracellular reduction of MTT and accumulation of insoluble formazan. After incubation, the MTT-containing media were fully removed, and the resulting formazan crystals were resolubilized via the addition of 200 µL of dimethyl sulfoxide (DMSO) to each well, followed by a 30-minute incubation at ambient temperature in the absence of light exposure. Quantitative absorbance readings were then obtained at a primary wavelength of 570 nm, with concurrent reference correction performed at 630 nm, utilizing a StatFax 2100 ELISA reader to ensure consistency and precision in optical density measurement. The recorded absorbance values served as numerical surrogates for cellular viability, proportional to intracellular enzymatic reduction capacity.

Statistical analysis

Statistical analyses were performed using R version 4.3.1. Data organization and visualization were conducted using the dplyr and ggplot2 packages, respectively. Distributional normality was evaluated using the Shapiro–Wilk test.

Differences among treatment conditions were assessed using one-way analysis of variance followed by Tukey's multiple-comparison procedure, with $p < 0.05$ considered statistically significant. Because $n = 24$ represented technical replicate wells from a single plate-based experimental run rather than independent biological experiments, the reported p-values describe within-experiment well-level differences and should be interpreted as exploratory.

Use of artificial intelligence-assisted tools

During preparation of this manuscript, the authors used ChatGPT (OpenAI) for English-language editing, consistency checking, and manuscript organization. The authors reviewed and verified all AI-assisted output and take full responsibility for the content of the manuscript.

Ethics approval

Although this study exclusively involved established immortalized cell lines and did not utilize human participants, patient-derived materials, or vertebrate animals, the research protocol underwent institutional review. The work was reviewed and approved by the Ethics Committee of North Khorasan University of Medical Sciences, which confirmed compliance with national and institutional biosafety and ethical standards for in-vitro cellular research. All experimental procedures were conducted in accordance with the approved protocol and relevant laboratory safety regulations.

Results

Direct NTP exposure and PAM treatment produced different MTT response patterns in U87-MG and L-929 cells. Longer direct NTP exposures reduced MTT absorbance in both cell lines, whereas PAM produced cell-line-dependent changes in MTT absorbance. Because MTT is an indirect measure of

metabolic activity, these findings do not independently demonstrate apoptosis, proliferation, selective tumor killing, or treatment safety.

Direct treatment results

Direct NTP exposure produced a duration-dependent change in MTT absorbance in L-929 fibroblast cells. The 30-s exposure did not differ from the untreated control (mean OD = 0.545, SD = 0.128; P = 0.628). In contrast, the 60- and 90-s exposures reduced MTT absorbance (60 s: mean OD = 0.245, SD = 0.155, $P = 1.8 \times 10^{-6}$; 90 s: mean OD = 0.221, SD = 0.150, $P = 9.7 \times 10^{-7}$). These Tukey-adjusted comparisons indicate reduced MTT-derived metabolic activity after prolonged exposure but do not establish apoptosis or another mechanism of cell death (Table 1 and Fig. 1).

U87-MG cells showed a similar duration-dependent MTT response. The 30-s exposure did not differ from the untreated control (mean OD = 0.495, SD = 0.152; P = 0.992), whereas the 60- and 90-s exposures reduced MTT absorbance (60 s: mean OD = 0.195, SD = 0.114, $P = 1.9 \times 10^{-7}$; 90 s: mean OD = 0.190, SD = 0.061, $P = 6.4 \times 10^{-9}$). These Tukey-adjusted comparisons demonstrate reduced MTT-derived metabolic activity following prolonged direct NTP exposure but do not confirm apoptosis or cell death (Table 1 and Fig. 2).

Table 1

MTT absorbance after direct NTP exposure. Values are mean OD ± SD from n = 24 technical wells per cell-line condition within one plate-based experimental run. P values versus the corresponding untreated control are from two-sided Tukey-adjusted comparisons following one-way ANOVA. The final column contains the reported between-cell-line P values; the exact test used for those values was not documented.

Treatment Duration	L-929 OD (Mean ± SD)	P value (vs control)	U87-MG OD (Mean ± SD)	P value (vs control)	Reported P value (L-929 vs U87-MG)
Control	0.547 ± 0.199	–	0.508 ± 0.196	–	–
Direct 30 s	0.545 ± 0.128	0.628	0.495 ± 0.152	0.992	0.364
Direct 60 s	0.245 ± 0.155	1.8×10 − 6	0.195 ± 0.114	1.9×10 − 7	0.009
Direct 90 s	0.221 ± 0.150	9.7×10 − 7	0.190 ± 0.061	6.4×10 − 9	0.984

Indirect (PAM) results

Compared with the vehicle control, L-929 cells showed higher MTT absorbance under all four tested PAM stock conditions: undiluted PAM stock (100%; mean OD = 0.675, SD = 0.200; P = 0.012), 50% (mean OD = 0.797, SD = 0.250; P = 0.0007), 25% (mean OD = 0.661, SD = 0.165; P = 0.0145), and 12.5% (mean OD = 0.774, SD = 0.165; P = 0.00015). These Tukey-adjusted comparisons indicate greater MTT-derived

metabolic activity but cannot be interpreted as increased proliferation without direct cell-counting or proliferation assays (Table 2 and Fig. 3).

In U87-MG cells, undiluted PAM stock (100%) reduced MTT absorbance relative to vehicle control (mean OD = 0.394, SD = 0.122; P = 0.038). The 50%, 25%, and 12.5% PAM stock conditions did not differ from vehicle control (P = 0.885, P = 0.902, and P = 0.599, respectively). Thus, only the undiluted PAM stock condition reduced U87-MG MTT-derived metabolic activity within this experimental run; apoptosis was not assessed (Table 2 and Fig. 4).

Table 2

MTT absorbance after PAM treatment. Values are mean OD ± SD from n = 24 technical wells per cell-line condition within one plate-based experimental run. P values versus the corresponding vehicle control are from two-sided Tukey-adjusted comparisons following one-way ANOVA. The final column contains the reported between-cell-line P values; the exact test used for those values was not documented.

PAM stock condition	L-929 OD (Mean ± SD)	P value (vs vehicle control)	U87-MG OD (Mean ± SD)	P value (vs vehicle control)	Reported P value (L-929 vs U87-MG)
Undiluted PAM stock (100%)	0.675 ± 0.200	0.012	0.394 ± 0.122	0.038	6.9×10 − 6
50% PAM stock condition	0.797 ± 0.250	0.0007	0.477 ± 0.118	0.885	2.1×10 − 6
25% PAM stock condition	0.661 ± 0.165	0.0145	0.489 ± 0.141	0.902	0.0007
12.5% PAM stock condition	0.774 ± 0.165	0.00015	0.500 ± 0.141	0.599	5.2×10 − 6

The reported well-level comparisons between L-929 and U87-MG cells showed different response patterns under the tested conditions. Following direct NTP exposure, the reported P values were 0.364 at 30 s, 0.009 at 60 s, and 0.984 at 90 s. At 60 s, mean MTT absorbance was 0.195 ± 0.114 in U87-MG cells and 0.245 ± 0.155 in L-929 cells. The reported between-cell-line P values for undiluted PAM stock (100%) and the 50%, 25%, and 12.5% PAM stock conditions were 6.9×10^{-6}, 2.1×10^{-6}, 0.0007, and 5.2×10^{-6}, respectively. Because the exact test that generated these Table 3P values was not documented and the comparisons used technical wells from a single run, they are exploratory and cannot establish biological selectivity (Table 3 and Fig. 5).

Table 3
Reported well-level comparisons of L-929 and U87-MG MTT absorbance. Values are mean OD ± SD from n = 24 technical wells per cell-line condition within one plate-based experimental run. The exact inferential test used to generate the reported between-cell-line P values was not documented in the available analysis record and must be confirmed before submission.

Treatment	L-929 OD (mean ± SD)	U87-MG OD (mean ± SD)	Reported P value
Direct 30 s	0.545 ± 0.128	0.495 ± 0.152	0.364
Direct 60 s	0.245 ± 0.155	0.195 ± 0.114	0.009
Direct 90 s	0.221 ± 0.150	0.190 ± 0.061	0.984
Undiluted PAM stock (100%)	0.675 ± 0.200	0.394 ± 0.122	6.9×10^{-6}
50% PAM stock condition	0.797 ± 0.250	0.477 ± 0.118	2.1×10^{-6}
25% PAM stock condition	0.661 ± 0.165	0.489 ± 0.141	0.0007
12.5% PAM stock condition	0.774 ± 0.165	0.500 ± 0.141	5.2×10^{-6}

Discussion

Under the tested in-vitro conditions, direct NTP and PAM produced distinct MTT response patterns in U87-MG and L-929 cells. Direct exposure for 60 and 90 s reduced MTT absorbance in both cell lines, whereas undiluted PAM stock (100%) reduced MTT absorbance in U87-MG cells and all four tested PAM stock conditions increased MTT absorbance in L-929 cells. These findings are exploratory because they derive from a single plate-based experimental run, use an immortalized murine fibroblast comparator rather than normal human brain cells, and rely on MTT absorbance rather than direct measurements of apoptosis or proliferation.

Direct NTP exposure produced a duration-dependent response in MTT absorbance. A 30-second exposure did not materially alter MTT absorbance in either cell line within this experimental run; however, this result does not establish a clinical safety margin. This pattern is consistent with previous reports suggesting that low-dose plasma can impose mild oxidative stress that cells may manage through endogenous antioxidant systems (15, 16). The reduced MTT absorbance observed at 60 and 90 seconds indicates diminished metabolic activity, but the present assay cannot determine whether apoptosis, necrosis, growth arrest, or another mechanism was responsible.

The marked reduction in MTT absorbance at 60 seconds in both L-929 cells (OD = 0.245) and U87-MG cells (OD = 0.195) indicates a decrease in metabolic activity in both cell lines. Although direct NTP can generate short-lived reactive oxygen and nitrogen species and physical factors such as UV photons and electromagnetic fields, these components were not quantified in the present study; therefore, their individual contributions cannot be determined from the current data.

Previous work indicates that direct NTP can generate short-lived reactive oxygen and nitrogen species together with physical components that may contribute to reduced cellular metabolic activity (17). However, these components and their downstream effects were not measured in the present experiment. At 60 seconds, U87-MG cells showed lower MTT absorbance than L-929 cells in the well-level comparison ($p = 0.009$), although both cell lines exhibited substantial reductions from their respective controls. This pattern indicates only a limited differential response under the tested condition and does not establish a therapeutic window. Previous studies have reported that direct plasma can induce DNA damage and mitochondrial dysfunction (18), but these outcomes were not measured here.

The reduced MTT absorbance observed after 60- and 90-second exposures is consistent with diminished cellular metabolic activity. However, because apoptosis, necrosis, DNA damage, lipid peroxidation, and cell-cycle arrest were not directly measured, the present data cannot determine the mechanism responsible for this reduction (19).

PAM produced different MTT response patterns in the two cell lines. Undiluted PAM stock (100%) reduced MTT absorbance in U87-MG cells, whereas all four tested PAM stock conditions increased MTT absorbance in L-929 cells (Table 2). Because L-929 is an immortalized murine fibroblast line and no independent biological experiments were performed, these observations should be described as differential cell-line responses rather than proof of cancer selectivity, normal-cell protection, or treatment safety. Previous studies have reported that low concentrations of reactive oxygen species can act as mitogenic signals and that differences in oxidative-stress responses, antioxidant capacity, and aquaporin expression may contribute to cell-dependent responses to PAM (9, 20–25). These mechanisms were not directly evaluated in the present study.

The mechanistic action of NTP extends beyond a simple increase in ROS, involving a sophisticated integration of molecular signaling and environmental interactions. Tanaka et al. showed that PAM selectively induces glioblastoma cell death through suppression of AKT kinase signaling (17). Also, molecular analyses reveal that PAM induces apoptosis in glioblastoma cells through the consistent upregulation of stress-inducible genes, including GADD45α, ATF3, c-JUN, and CDKN1A. These reactive species trigger a cytokine-mediated GADD45α/p38 pathway, which elevates transcription factor levels to drive programmed cell death. Furthermore, the treatment significantly upregulates key genes such as CHAC1, IER3, and RND3, which are associated with growth inhibition and increased sensitivity to apoptosis. This process is further regulated by a negative feedback loop involving the activator protein 1 (AP-1) complex and dual-specificity phosphatase (DUSP) family genes, which serve to downregulate MAPK signaling following the initial oxidative insult (25).

Reported differential responses depend not only on malignant versus normal status but also on cell type and experimental context. Nutrient availability can shape these responses: nutrient-starved environments can enhance intracellular ROS accumulation and sensitize glioblastoma cells, whereas nutrient-rich conditions may allow fibroblasts to buffer oxidative eustress and maintain or increase metabolic activity (26).

The vulnerability of U87-MG cells to PAM may be linked to their metabolic reprogramming (the Warburg effect). Glioblastoma cells predominantly utilize glycolysis for energy production, even in the presence of oxygen. PAM treatment has been shown to disrupt this glycolytic flux, depleting intracellular adenosine triphosphate (ATP) and oxidized nicotinamide adenine dinucleotide (NAD^+) levels, which are critical for DNA repair and cellular maintenance. By forcing a metabolic shift and depleting energy reserves, PAM renders U87-MG cells unable to maintain membrane integrity or repair oxidative damage (27).

Glioblastoma is notoriously difficult to treat because of the BBB and its highly infiltrative growth pattern, which precludes complete surgical resection from serving as an adequate curative strategy (28–30). While direct plasma treatment is limited by the need for surgical exposure, the liquid-based nature of PAM motivates further investigation of locoregional routes such as direct injection into the resection cavity or convection-enhanced delivery; the present in-vitro study did not evaluate delivery feasibility or efficacy. The mechanistic efficacy of cold plasma devices involves enhancing the potency of established chemotherapeutic agents like temozolomide; these devices have demonstrated improved survival in glioblastoma xenograft models and antitumor effects independent of chemical species, highlighting their potential as non-invasive adjuncts to surgery and systemic therapies (31, 32).

Although the present single-run findings indicate different MTT response patterns between U87-MG and L-929 cells, variability among glioblastoma cell lines, including the resistance frequently reported in T98G relative to U87-MG, requires broader evaluation. T98G cells, for instance, possess different p53 and PTEN mutation profiles from U87-MG cells, which may contribute to greater antioxidant capacity and resistance to ROS-mediated apoptosis. Future studies should evaluate plasma-treatment responses across glioblastoma models with different genetic and metabolic profiles (33).

Although L-929 cells provide a fibroblast comparator, they are not a validated model of normal human neural tissue and cannot establish neuro-safety. Primary human astrocytes, neurons, brain endothelial cells, pericytes, and other relevant human brain-cell controls should be evaluated in future studies. In-vivo studies using orthotopic xenograft models will also be required to assess whether biologically active PAM exposures can be achieved within the brain without inducing neurotoxicity or inflammation.

A strength of this study is its direct comparative design, in which direct non-thermal plasma exposure and PAM treatment were evaluated under a unified in-vitro framework using the same cell-culture conditions, endpoint timing, and viability assay. The use of graded direct exposure durations and the four PAM stock conditions allowed the identification of distinct within-experiment response patterns between the two approaches. The inclusion of a matched vehicle control and 24 technical replicate wells per condition improved the precision of within-experiment measurements; however, technical replicates do not replace independent biological replication. The study therefore provides preliminary data to guide future mechanistic, chemically characterized, and preclinical investigations.

This study has several important limitations. First, all findings were obtained from a single plate-based experimental run with 24 technical replicate wells per condition and no independent experiments performed on different days. Consequently, the inferential statistics reflect within-experiment well-level

variation and do not establish reproducibility across biological experiments. Second, MTT absorbance is an indirect measure of metabolic activity and cannot alone establish apoptosis, proliferation, clonogenic survival, or a specific mechanism of cell death. Third, PAM was not chemically characterized for pH, conductivity, osmolality, oxidation–reduction potential, hydrogen peroxide, nitrite, or nitrate. The liquid-surface temperature was monitored during treatment, and no measurable reduction in liquid volume occurred following either 5 or 10 minutes of plasma exposure. However, the absence of quantitative physicochemical characterization limits mechanistic interpretation of the observed responses. Additional controls, including sham plasma exposure, pH-matched controls, osmolality-matched controls, synthetic reactive-species controls, and positive cytotoxic controls, were not included. Finally, the use of L-929 murine fibroblasts does not establish selectivity or safety in normal human neural tissue.

Conclusion

In conclusion, under the tested single-run in-vitro conditions, direct NTP exposure for 60 and 90 s reduced MTT-derived metabolic activity in both U87-MG glioblastoma and L-929 fibroblast cells. PAM produced a different response pattern: undiluted PAM stock (100%) reduced MTT absorbance in U87-MG cells, whereas all four tested PAM stock conditions increased MTT absorbance in L-929 cells. These findings support further investigation of PAM but do not demonstrate selective eradication of glioblastoma cells, apoptosis, proliferation, treatment safety, therapeutic efficacy, or a therapeutic index. Confirmation will require independent biological replication, quantitative PAM characterization, verified plasma dosimetry, appropriate human neural controls, mechanistic assays, and in-vivo evaluation.

Declarations

Acknowledgements

The authors acknowledge the Institute of Biotechnology at Ferdowsi University of Mashhad for providing the cell lines, the Plasma Physics Laboratory staff for technical assistance with the plasma device, and laboratory personnel at North Khorasan University of Medical Sciences for logistical support.

Funding

This research was funded by North Khorasan University of Medical Sciences, with the funding received by Amir Rahmanian Sharifabad.

Author contributions

E.S.M.: Investigation, Methodology, Writing—original draft. M.R.: Formal analysis, Data curation, Writing—original draft, Writing—review & editing. F.O.: Investigation, Methodology, Writing—review & editing. R.F.: Conceptualization, Methodology, Writing—review & editing. S.K.: Visualization, Writing—review & editing.

S.M.K.: Investigation, Resources, Writing—review & editing. A.R.S.: Writing—review & editing. All authors reviewed and approved the final manuscript.

Data availability

The well-level data and analysis code underlying all figures and tables are not publicly deposited but are available from the corresponding author on reasonable request.

Competing interests

The authors declare no competing interests.

References

1. Tamimi, A. F. & Juweid, M. Chapter 8: epidemiology and outcome of glioblastoma. *Glioblastoma NCBI Bookshelf* (2017).
2. Loras, A., Gonzalez-Bonet, L. G., Gutierrez-Arroyo, J. L., Martinez-Cadenas, C. & Marques-Torrejon, M. A. Neural stem cells as potential glioblastoma cells of origin. *Life* **13** (4), 905 (2023).
3. Ng, A. T. et al. The challenges and clinical landscape of glioblastoma immunotherapy. *CNS Oncol.* **13** (1), 2415878 (2024).
4. Singh, S. et al. Glioblastoma at the crossroads: current understanding and future therapeutic horizons. *Signal. Transduct. Target. Therapy*. **10** (1), 213 (2025).
5. Lin, A. et al. Non-Thermal Plasma as a Unique Delivery System of Short-Lived Reactive Oxygen and Nitrogen Species for Immunogenic Cell Death in Melanoma Cells. *Adv. Sci.* **6** (6), 1802062 (2019).
6. Min, T. et al. Therapeutic Effects of Cold Atmospheric Plasma on Solid Tumor. *Front. Med.* **9**, 884887 (2022).
7. Zhang, M., Yang, D., Meng, X., Liu, Y. & Zhang, T. A Review on the Application and Mechanism of Low Temperature Plasma in the Field of Tumor Therapy. *Technol. Cancer Res. Treat.* **24**, 15330338251356439 (2025).
8. Faramarzi, F. et al. Cold physical plasma in cancer therapy: mechanisms, signaling, and immunity. *Oxidative Med. Cell. Longev.* **2021** (1), 9916796 (2021).
9. Yan, D., Sherman, J. H. & Keidar, M. Cold atmospheric plasma, a novel, promising anti-cancer treatment modality. *Oncotarget* **8** (9), 15977 (2016).
10. Bauer, G., Sersenová, D., Graves, D. B. & Machala, Z. Cold Atmospheric Plasma and Plasma-Activated Medium Trigger RONS-Based Tumor Cell Apoptosis. *Sci. Rep.* **9** (1), 14210 (2019).
11. Yan, D. et al. Cold atmospheric plasma cancer treatment, a critical review. *Appl. Sci.* **11** (16), 7757 (2021).
12. Saadati, F. et al. Comparison of Direct and Indirect cold atmospheric-pressure plasma methods in the B16F10 melanoma cancer cells treatment. *Sci. Rep.* **8** (1), 7689 (2018).

13. Fan, R. et al. Properties and anticancer effects of plasma-activated medium stored at different temperatures. *AIP Adv.* **12** (9), 095022 (2022).
14. von Woedtke, T., Bekeschus, S., Weltmann, K. D. & Wende, K. Plasma-Treated Liquids for Medicine: A Narrative Review on State and Perspectives. *Plasma Processes Polym.* **22** (1), 2400255 (2025).
15. Abdo, A. I. & Kopecki, Z. Comparing redox and intracellular signalling responses to cold plasma in wound healing and cancer. *Curr. Issues. Mol. Biol.* **46** (5), 4885–4923 (2024).
16. Kalghatgi, S. U. et al. Mechanism of blood coagulation by nonthermal atmospheric pressure dielectric barrier discharge plasma. *IEEE Trans. Plasma Sci.* **35** (5), 1559–1566 (2007).
17. Tanaka, H. et al. Plasma-activated medium selectively kills glioblastoma brain tumor cells by down-regulating a survival signaling molecule, AKT kinase. *Plasma Med.* **1**, 3–4 (2011).
18. Kim, G., Kim, W., Kim, K. & Lee, J. DNA damage and mitochondria dysfunction in cell apoptosis induced by nonthermal air plasma. *Appl. Phys. Lett.* ;**96**(2). (2010).
19. Lunov, O. et al. Chemically different non-thermal plasmas target distinct cell death pathways. *Sci. Rep.* **7** (1), 600 (2017).
20. Kalghatgi, S., Friedman, G., Fridman, A. & Clyne, A. M. Endothelial cell proliferation is enhanced by low dose non-thermal plasma through fibroblast growth factor-2 release. *Ann. Biomed. Eng.* **38** (3), 748–757 (2010).
21. Arjunan, K. P., Friedman, G., Fridman, A. & Clyne, A. M. Non-thermal dielectric barrier discharge plasma induces angiogenesis through reactive oxygen species. *J. R Soc. Interface*. **9** (66), 147–157 (2012).
22. Lee, C. B. et al. Enhancing antitumor immunity in Lewis lung cancer through plasma-treated medium-induced activation of dendritic cells. *Cancer Cell Int.* **24** (1), 389 (2024).
23. Tomić, S. et al. Plasma-Activated Medium Potentiates the Immunogenicity of Tumor Cell Lysates for Dendritic Cell-Based Cancer Vaccines. *Cancers [Internet]*. **13** (7), 1626 (2021).
24. Yao, H. et al. Anti-Tumor Effect of Non-Thermal Atmospheric Pressure Plasma-Activated Medium on Synovial Sarcoma: An In Vitro and In Vivo Study. *Biomedicines [Internet]*. **13** (3), 534 (2025).
25. Tanaka, H. et al. Oxidative stress-dependent and-independent death of glioblastoma cells induced by non-thermal plasma-exposed solutions. *Sci. Rep.* **9** (1), 13657 (2019).
26. Yan, D. et al. The specific vulnerabilities of cancer cells to the cold atmospheric plasma-stimulated solutions. *Sci. Rep.* **7** (1), 4479 (2017).
27. Kurake, N. et al. Non-thermal plasma-activated medium modified metabolomic profiles in the glycolysis of U251SP glioblastoma. *Arch. Biochem. Biophys.* **662**, 83–92 (2019).
28. Rahmanian, M., Oroojalian, F., Kesharwani, P. & Sahebkar, A. Liposome-mediated anticancer drug delivery strategies for advancing brain tumor therapy. *Eur. Polymer J.* **233**, 114001 (2025).
29. Rahmanian, M., Oroojalian, F., Kesharwani, P. & Sahebkar, A. Current trends in triblock copolymer-based multifunctional nanotheranostics for cancer treatment. *J. Drug Deliv. Sci. Technol.* **99**, 105985 (2024).

30. Zandsalimi, F., Aghamiri, S., Roshanzamiri, S., Shahmohamadnejad, S. & Ghanbarian, H. The emerging role of cold atmospheric plasma in glioblastoma therapy. *Plasma Processes Polym.* **17** (10), 1900189 (2020).
31. Akter, M., Lim, J. S., Choi, E. H. & Han, I. Non-Thermal Biocompatible Plasma Jet Induction of Apoptosis in Brain Cancer Cells. *Cells* ;**10**(2). (2021).
32. Yao, X. et al. Cold plasma discharge tube enhances antitumoral efficacy of temozolomide. *ACS Appl. Bio Mater.* **5** (4), 1610–1623 (2022).
33. Tanaka, H. et al. Glioblastoma cell lines display different sensitivities to plasma-activated medium. *IEEE Trans. Radiation Plasma Med. Sci.* **2** (2), 99–102 (2017).

Figures

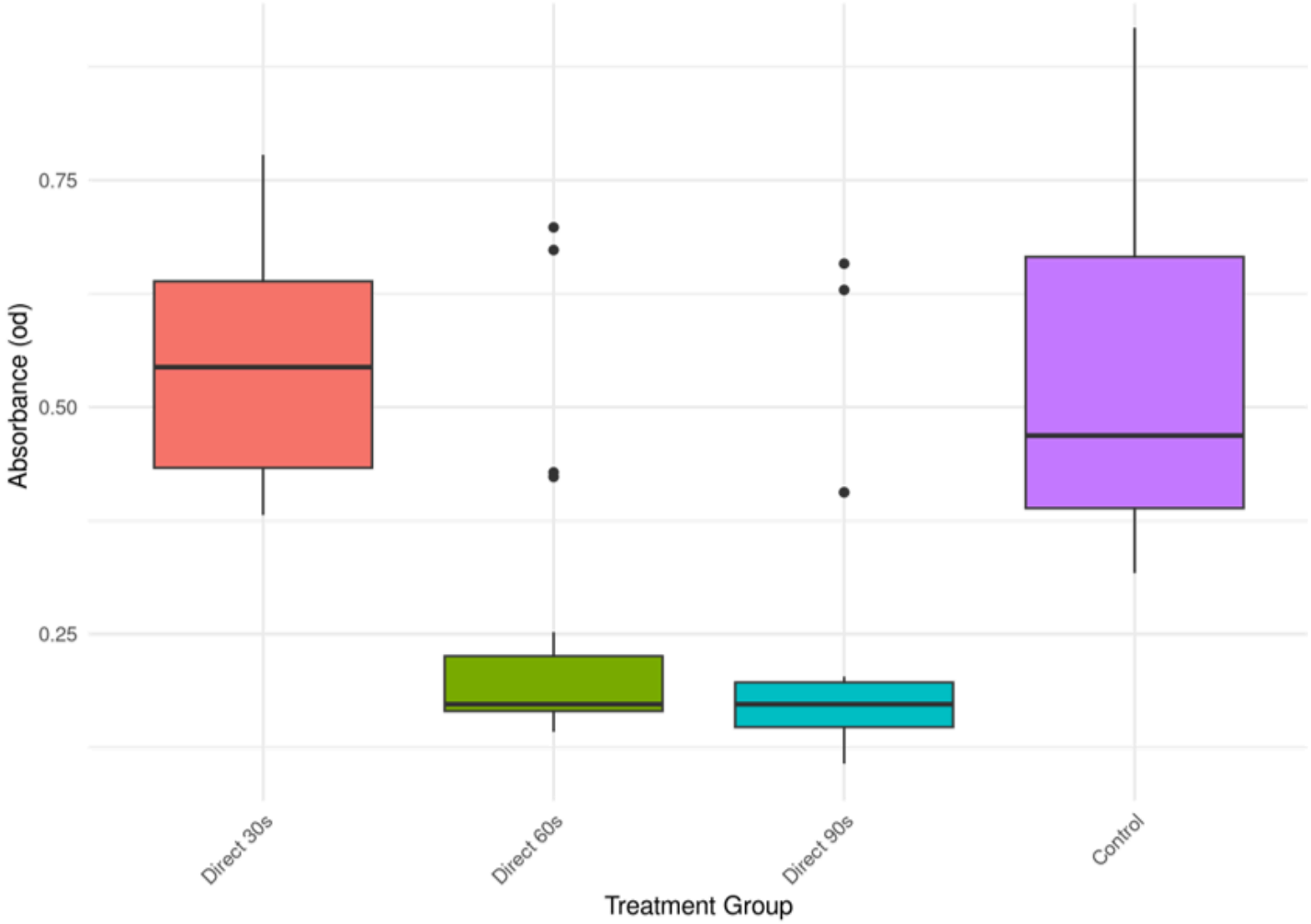


Figure 1

Direct NTP exposure in L-929 cells. Boxplots show MTT absorbance for the untreated control and 30-, 60-, and 90-s direct NTP exposures. Each condition contains n = 24 technical wells from one plate-based

experimental run. Boxes show the interquartile range, centre lines show the median, whiskers extend to 1.5 times the interquartile range, and points beyond the whiskers are plotted individually. One-way ANOVA followed by two-sided Tukey-adjusted comparisons with the control was used; exact P values are given in Table 1. NTP, non-thermal plasma; OD, optical density.

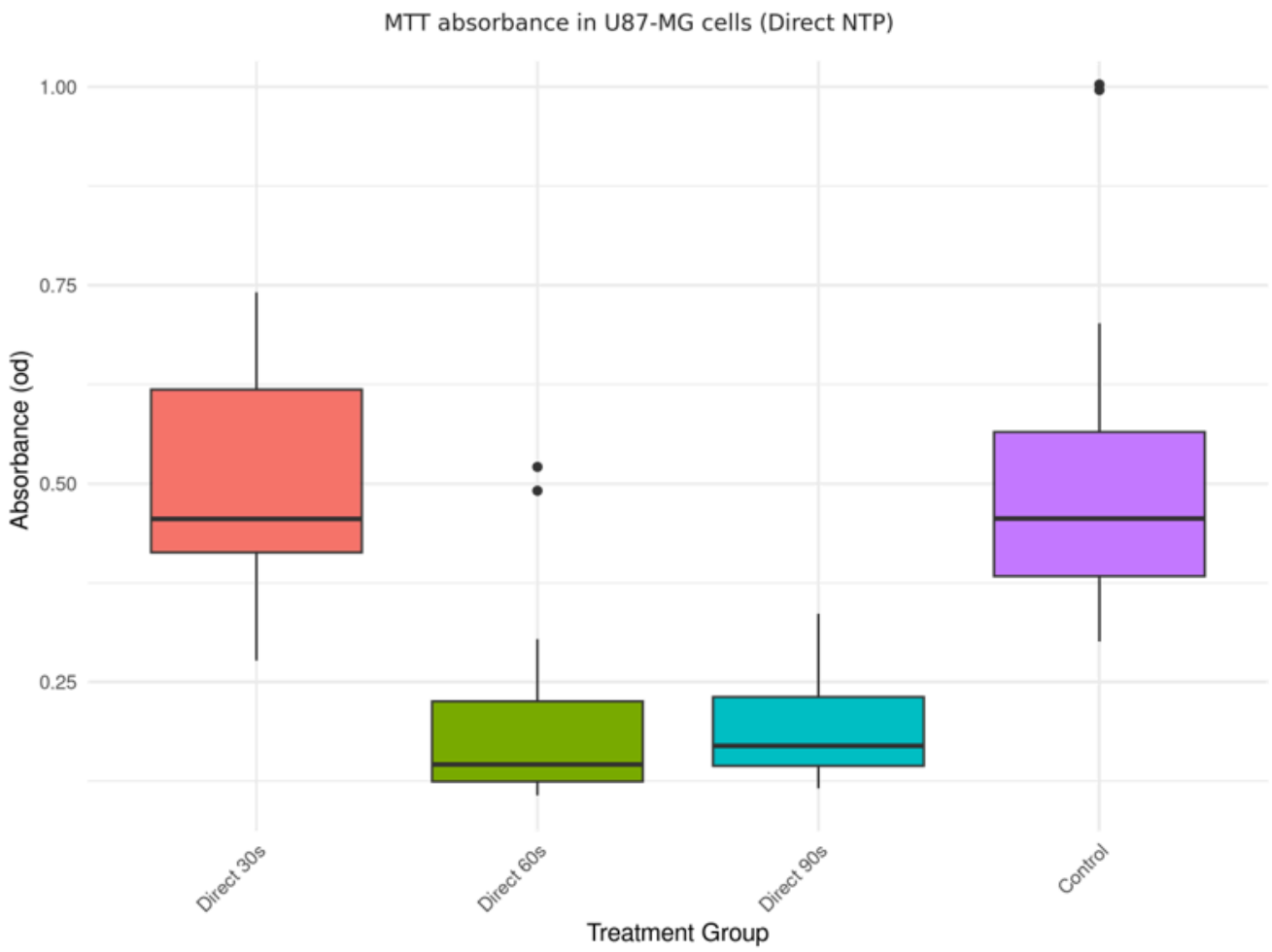


Figure 2

Direct NTP exposure in U87-MG cells. Boxplots show MTT absorbance for the untreated control and 30-, 60-, and 90-s direct NTP exposures. Each condition contains n = 24 technical wells from one plate-based experimental run. Boxes show the interquartile range, centre lines show the median, whiskers extend to 1.5 times the interquartile range, and points beyond the whiskers are plotted individually. One-way ANOVA followed by two-sided Tukey-adjusted comparisons with the control was used; exact P values are given in Table 1. NTP, non-thermal plasma; OD, optical density.

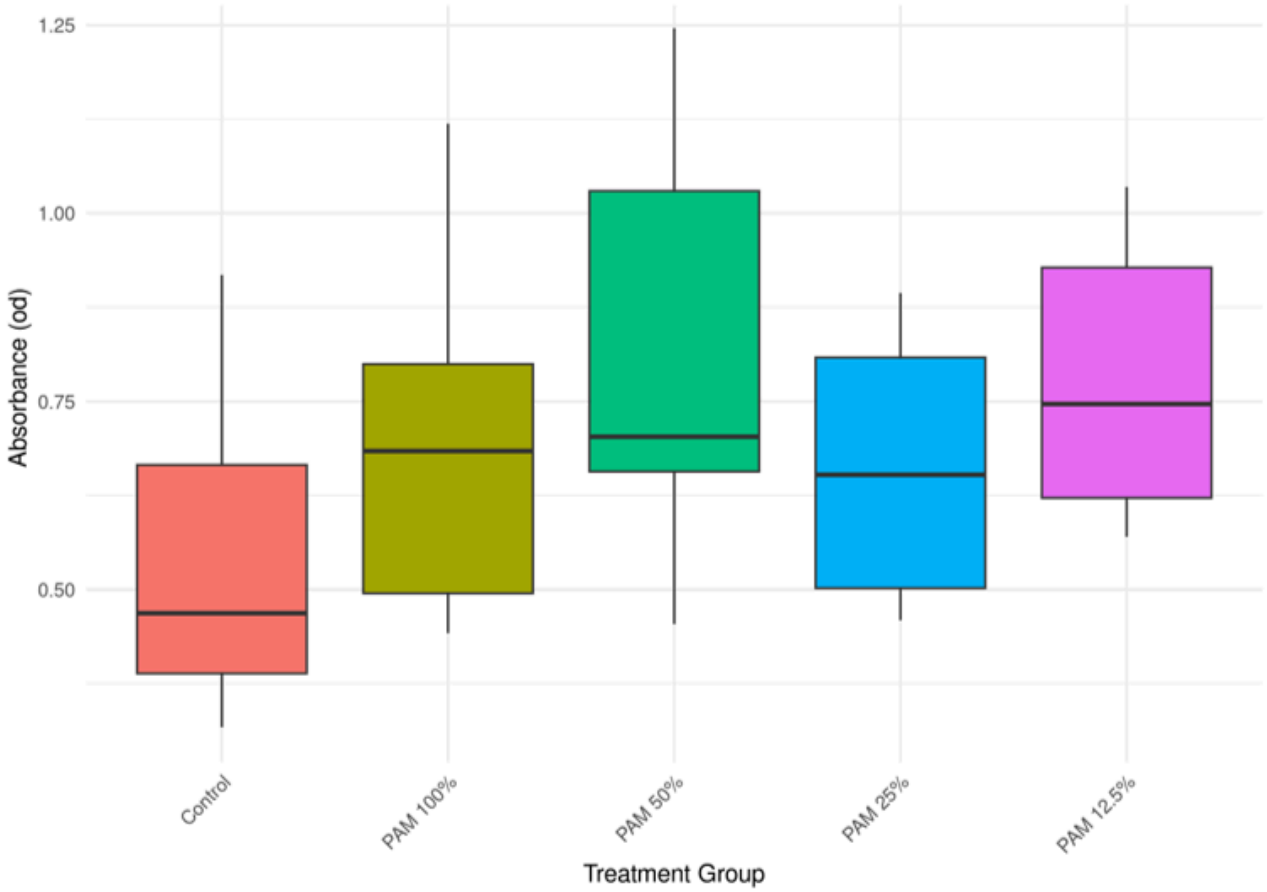


Figure 3

PAM treatment in L-929 cells. Boxplots show MTT absorbance for the vehicle control, undiluted PAM stock (100%), and the 50%, 25%, and 12.5% PAM stock conditions. Each condition contains n = 24 technical wells from one plate-based experimental run. All four tested PAM conditions had higher MTT absorbance than vehicle control; exact Tukey-adjusted P values are given in Table 2. Boxes show the interquartile range, centre lines show the median, whiskers extend to 1.5 times the interquartile range, and points beyond the whiskers are plotted individually. PAM, plasma-activated medium; OD, optical density.

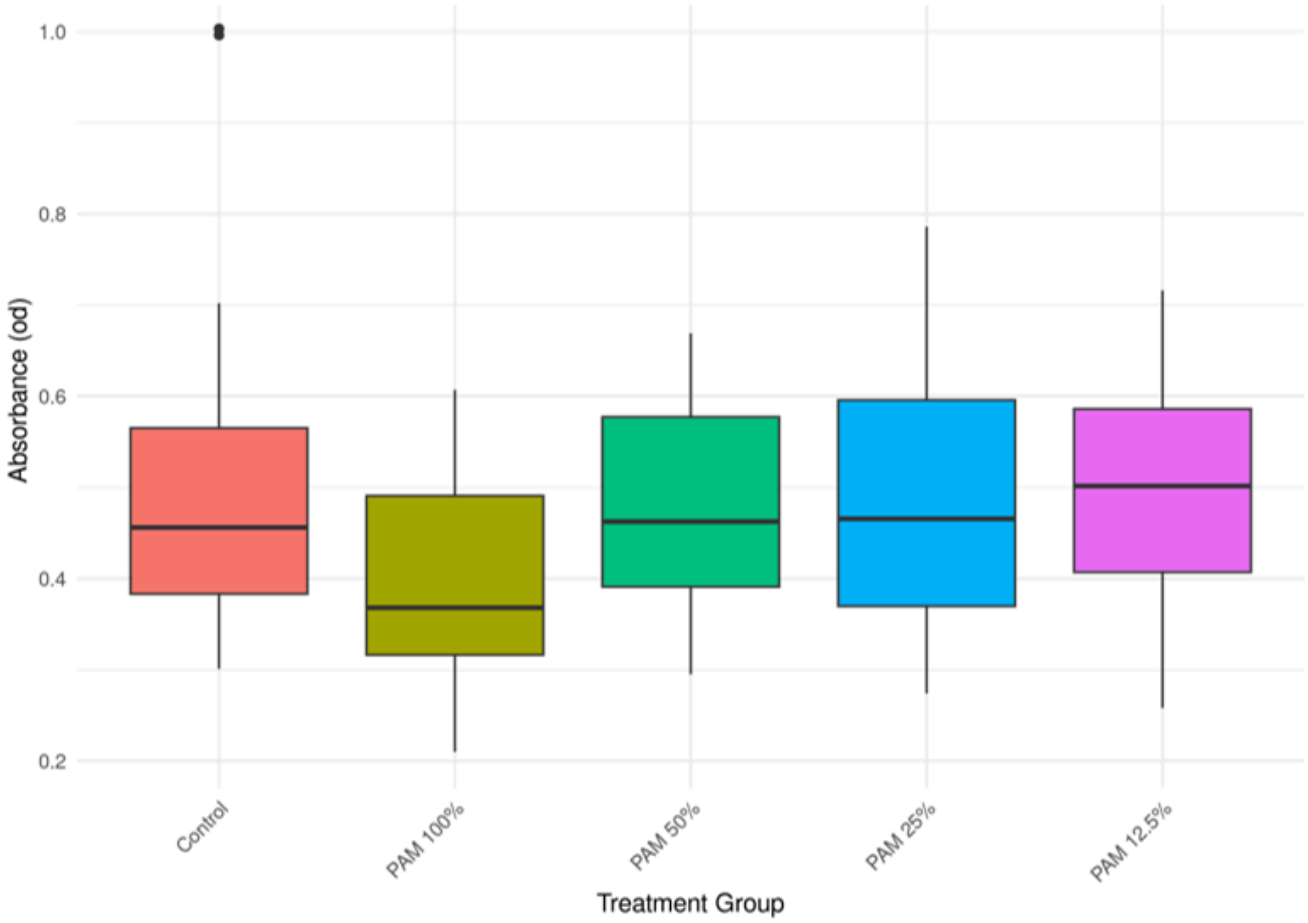


Figure 4

PAM treatment in U87-MG cells. Boxplots show MTT absorbance for the vehicle control, undiluted PAM stock (100%), and the 50%, 25%, and 12.5% PAM stock conditions. Each condition contains n = 24 technical wells from one plate-based experimental run. One-way ANOVA followed by two-sided Tukey-adjusted comparisons with the vehicle control was used; exact P values are given in Table 2. Boxes show the interquartile range, centre lines show the median, whiskers extend to 1.5 times the interquartile range, and points beyond the whiskers are plotted individually. PAM, plasma-activated medium; OD, optical density.

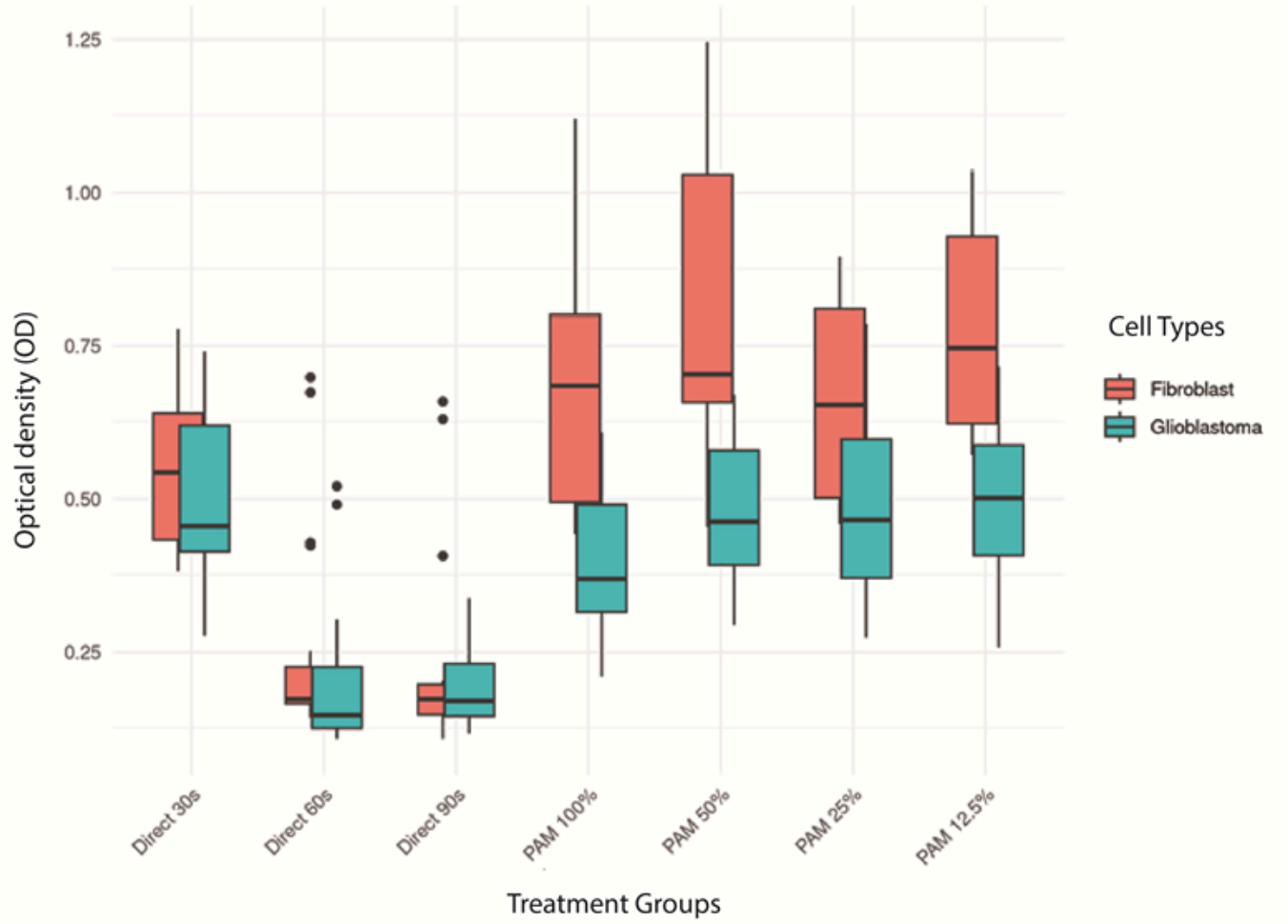


Figure 5

Well-level comparison of L-929 and U87-MG MTT absorbance. Boxplots compare the two cell lines after 30-, 60-, and 90-s direct NTP exposures and after treatment with undiluted PAM stock (100%) or the 50%, 25%, and 12.5% PAM stock conditions. Each cell-line condition contains n = 24 technical wells from one plate-based experimental run. Boxes show the interquartile range, centre lines show the median, whiskers extend to 1.5 times the interquartile range, and points beyond the whiskers are plotted individually. Reported between-cell-line P values are given in Table 3; the exact inferential test used to generate them was not documented in the available analysis record. NTP, non-thermal plasma; PAM, plasma-activated medium; OD, optical density.

Supplementary Files

This is a list of supplementary files associated with this preprint. Click to download.

- GA.png